Medium-scale experiment in consolidation of an artificial sea ice ridge in Van Mijenfjorden, Svalbard

Evgenii Salganik [a,b], Knut Vilhelm Høyland [a,*], Aleksey Shestov [b]

[a] *Department of Civil and Environmental Engineering, Norwegian University of Science and Technology, Trondheim, Norway*
[b] *The University Centre in Svalbard, Longyearbyen, Norway*

ARTICLE INFO

ABSTRACT

This study characterizes a consolidation of undeformed level ice and ice ridges. Field investigations were performed in the Van Mijenfjorden, Svalbard for 66 days between February and May of 2017. The thickness and properties of the level ice that was used to make the ridge were measured, and thermistor-strings were installed in the ridge and the neighboring level ice. The ridge was visited four times for drilling and sampling. During our field experiment, the level ice (LI) grew from 50 to 99 cm, the consolidated layer (CL) grew up to 120 cm, and the ridge initial macroporosity was about 0.36. The experimental results provided enough information for accurate growth prediction and validation of ridge consolidation models.

Two analytical resistive models and two-dimensional discretized numerical models are presented. All models need general met-ocean conditions and general ice physical properties. The ridge model includes the effect of the inhomogeneous top and bottom surfaces of the consolidated layer. The models were validated against the field measurements, and the further details of the analytical models were validated against the numerical model.

The analytical resistive ridge model with convective atmospheric flux captures the relevant phenomena well and could be used for prediction of the consolidated layer thickness in probabilistic analysis of ice actions on structures. The model including the radiative terms predicted heat fluxes in level ice and ridge better than the convective model but required more input data. Vertical temperature profiles through the consolidated layer and further into respectively a void and an ice block may result in significantly different estimations of the consolidated layer thickness. The difference between fresh and saline ice growth is becoming significant only during the warming phase due to significant change of sea ice microporosity.

1. Introduction

According to the definition of the World Meteorological Organization (WMO Sea-Ice Nomenclature, 1971), an ice ridge is a line or wall of broken ice forced up by pressure. Ridges usually consist of three parts: the sail, the consolidated layer, and the unconsolidated rubble. The thickness of level ice, the consolidated layer, and the keel depth are the main ridge parameters for ice action calculations. The level ice h_i and the consolidated layer h_c thicknesses can be measured by mechanical or thermal drilling or from the ridge vertical temperature profile. Experiments are costly and time-consuming. It is beneficial if h_i and h_c can be predicted based on models with general met-ocean data as input. Simple analytical models have the advantage of being applicable in the probabilistic approach for ice action and evaluation of structural reliability.

Advanced numerical models for ridge consolidation exist (Høyland, 2002a; Marchenko, 2008), but these are difficult to use in probabilistic design where for example different climate scenarios need to be considered and thousands of simulations should be run to quantify structural reliability. The traditional solution is based upon modifying the latent heat in Stefan's law with the rubble macro-porosity (Lep-päranta and Hakala, 1992). In the simplest form, this solution neither takes into account the snow cover nor the atmospheric boundary layer (the air), but modifications to include these can easily be done. However, the effects of the real three-dimensional bottom and top surfaces of the consolidated layer are not included.

A few field studies describe the seasonal development of consolidated layer (Blanchet, 1998; Høyland, 2007; Shestov et al., 2018), and only one field study (Leppäranta et al., 1995) report observations of formation date and initial conditions. In basin-scale experiments on ridge consolidation (Høyland et al., 2001; Salganik and Høyland, 2018;
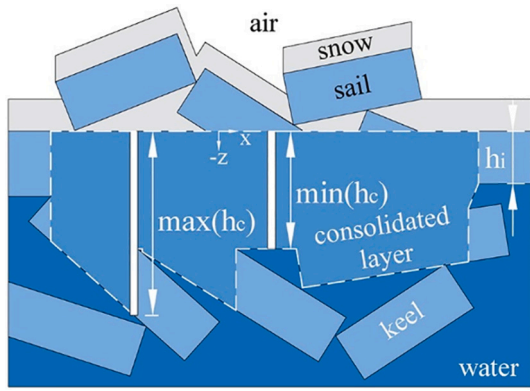

Fig. 1. Ice ridge cross-section with a boundary of the consolidated layer (white dashed line) and its maximum and minimum thickness h_c, surrounded with a level ice with thickness h_i.

Timco and Goodrich, 1988) the initial conditions can be quantified, but it is not straight forward to up-scale them to full-scale conditions. Basins are often indoors and have no snow and different ratios between the different atmospheric fluxes. Small-scale consolidation is usually controlled by turbulent fluxes, while large-scale thermodynamics mainly depends on longwave and shortwave radiation. There are also size effects (Salganik et al., 2020), and this means that ridge consolidation includes a large range of scales and ratios of thermal resistances.

The consolidation process of ice ridge is usually characterized by the ratio $R = h_c/h_i$ of thicknesses, the consolidated layer to level ice. The natural ridging process can occur at any time throughout the season. Ridge consolidation description using factor R is practical for engineering purposes, but not helpful for consolidation model validation. The factor R is sensitive to the initial level ice thickness at the time of ridge formation. In this paper thickness of the consolidated layer h_c is defined as a minimum of newly formed ice between ice blocks (Fig. 1).

Medium-scale consolidation experiments provide the advantage of accurately measured parameters such as initial macroporosity, initial block temperature, and salinity, and freezing time, which are normally not available in case of full-scale natural ridges. It reduces error in crucial parameters for the consolidation process, which includes

radiation, air natural, and forced convection, conduction through snow and ice, and phase change. Saline ice has a polycrystalline structure with salt brine inclusions between crystals. Thus, any temperature or salinity change leads to the change of sea ice solid fraction. In this paper, we define and validate a simple analytical consolidation model suitable for transient air temperature, wind speed, and snow thickness. The field experiment was intended to compare thermodynamics and development of physical and mechanical parameters of level ice and consolidated layer.

2. Sea ice growth modelling

2.1. Basic assumptions and atmospheric fluxes

We have used two analytical and two numerical models to calculate the growth and thickness of level ice and the consolidated layer. The analytical models are one-dimensional, and they ignore thermal inertia. The two-dimensional numerical models were used to estimate the error from these simplifications. All models require the following input of material and morphological parameters:

- Snow: thickness, thermal conductivity (Calonne et al., 2011).
- Level ice: salinity and thickness.
- Ridges: macroporosity; block initial temperature, salinity, and thickness; sail size, consolidated layer salinity, and thickness.

The heat exchange with the atmosphere must be estimated and this was modelled in two ways. Firstly, with a simple convective flux, and secondly, with a more advanced model including radiation and turbulence (Maykut, 1986).

In the convective model the atmospheric flux q_{atm} is given as:

$$q_{atm} = H_{ia}(T_{as} - T_a) \tag{1}$$

where T_{as} is the air-snow interface temperature, T_a is the air ambient temperature, and the convective heat transfer coefficient H_{ia} is a function of only the wind speed V_w and can be found as (Adams et al., 1960):

$$H_{ia} = max\left(11.6, 5.7V_w^{0.8}\right) \tag{2}$$

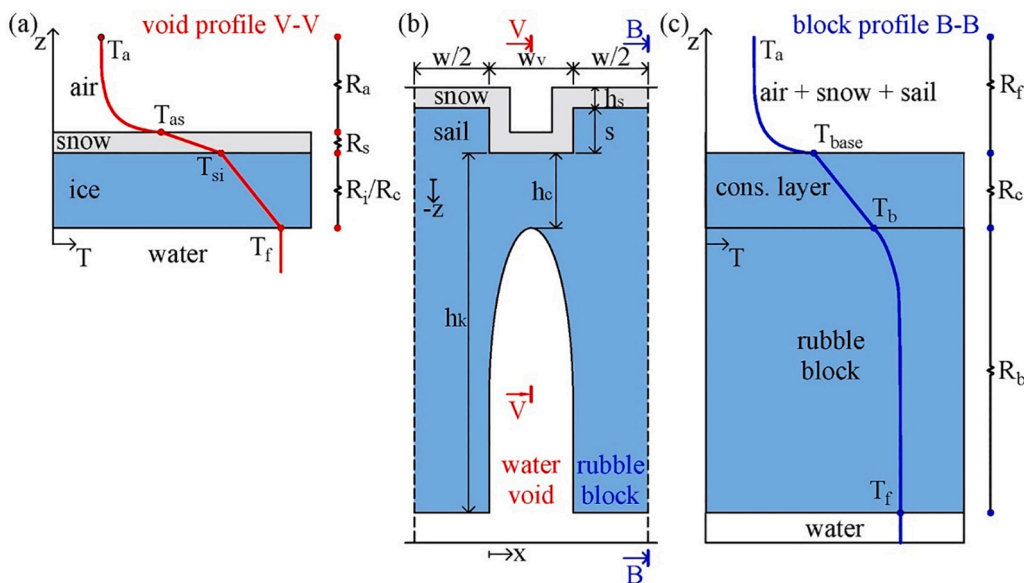The radiative model is more complicated and includes longwave and

Fig. 2. Sketch of geometry used in analytical and numerical models of a ridge, w is the block width, w_v is the void width, h_s is the snow thickness, s is the sail height, h_k is the keel depth, and h_c the minimum thickness of the consolidated layer (b) and thermal resistance model for the level ice and ridge void (a), and for the ridge block (c).

shortwave radiation, sensible and latent heat fluxes. Radiation fluxes are not simply proportional to the difference between surface and air ambient temperatures $T_{as} - T_a$ and cannot be simply included in the total model in the form of temperature-independent resistance as for convective model. It requires the following meteorological data:

- LW radiation: air temperature, humidity, cloudiness (Rosati and Miyakoda, 1988).
- SW radiation: cloudiness, surface albedo (Shine, 1984).
- Turbulent fluxes: air temperature, wind speed (Smith, 1988).

The net surface heat flux can be written as (Maykut, 1986):

$$q_{LW} + q_{SW} + q_s + q_e + q_m + q_c = 0 \tag{3}$$

where q_{LW} is the net longwave radiation, q_{SW} is the net shortwave radiation, q_s is the sensible heat flux, q_e is the latent heat flux, q_m is the top surface melting heat flux, q_c is the conductive flux through the ice and snow. Details on how to calculate the different fluxes are given in Appendix A. The equilibrium snow top surface temperature T_{as} can be found numerically from Eq. (3), and the conductive flux up through the ice and the snow can be found as:

$$q_c = \frac{k_s k_i}{k_s h_i + k_i h_s} \left(T_f - T_{as} \right) \tag{4}$$

where k_s and k_i are the snow and ice thermal conductivities, h_s and h_i are the snow and ice thicknesses, T_f is the water freezing temperature.

2.2. Analytical 1-D resistive level ice model

With this model, the growth of level ice with a uniform snow cover in steady-state conditions can be simulated with a convective atmospheric flux. The growth depends on how the temperature difference between air and water is distributed between insulating layers of air, snow, and ice. For slow changes of boundary conditions, the temperature gradient at the bottom of ice depends on the ice top surface temperature and its thickness. Three thermal resistances define temperature profile: air R_a, snow R_s and ice R_i (Fig. 2a).

The total system thermal resistance is showing how much heat can be transported in time from the water to the air. To find the vertical heat flux q at any time one should know air and water temperatures T_a and T_f, and the values defining three thermal resistances namely snow thickness h_s and thermal conductivity k_s, ice thickness h_i and thermal conductivity k_i, and convective heat transfer coefficient H_{ia}:

$$q = \frac{T_a - T_{as}}{R_a} = \frac{T_{as} - T_{si}}{R_s} = \frac{T_{si} - T_f}{R_i} = \frac{T_a - T_f}{R_a + R_s + R_i} \tag{5}$$

$$R_a = 1/H_{ia} \tag{6}$$

$$R_s = h_s/k_s \tag{7}$$

$$R_i = h_i/k_i \tag{8}$$

where T_{as} and T_{si} are the air-snow and snow-ice interface temperatures.

Convective heat transfer coefficient H_{ia} can be estimated from the measured wind speed from Eq. (2), the snow thermal conductivity depends on snow density (Calonne et al., 2011), ice thermal conductivity slightly depends on its salinity and temperature (Schwerdtfeger, 1963), and the snow and ice thicknesses and should be measured manually or estimated from the measured vertical temperature profiles. The more advanced radiative model described in Section 2.1 has been also used in this analytical resistive model.

Level ice thickness can be accurately estimated from the vertical temperature profile. Ice thermal conductivity development can be estimated from its temperature and periodically measured salinity profiles.

There is only a very weak dependence of drift snow and depth hoar

temperature on its thermal conductivity (Sturm et al., 1997). In our paper we suggest estimating snow thermal conductivity values from the measured snow thickness and vertical temperature profile in snow and ice as:

$$k_s = \frac{\left(T_{si} - T_f \right)}{\left(T_{as} - T_{si} \right)} \frac{k_i h_s}{h_i} \tag{9}$$

One of the ways to validate this model is to compare the estimated and measured interface temperatures. In transient conditions, temperature distribution will be following described ratios with a time lag defined by the thermal inertia of snow and ice. Higher time lag will be corresponding to the higher thermal resistance of layers above the chosen level of temperature measurements.

The analytical resistive model with convective or radiative atmospheric flux can be used for ice growth estimation based on the knowledge of air and water temperature, ice and snow thickness and thermal conductivity, and wind speed. The results of these predictions can be validated using manually measured ice thickness. Assuming no oceanic flux from the water and no thermal inertia, the pure ice growth can be estimated as:

$$\rho_i L_i dh_i/dt = -k_i \partial T/\partial z \tag{10}$$

where ρ_i is the density of fresh ice, L_i is the specific latent heat of ice, t is the time.

Gas-free fresh (pure) ice growth can be estimated from meteorological data including air temperature, wind speed, and snow thickness as:

$$\rho_i L_i \frac{dh_i}{dt} = \frac{T_f - T_a}{R_a + R_s + R_i} \tag{11}$$

Sea ice is saline and has different thermal properties and corresponding thermal response. However, the major difference is related to melting and the difference in the growth of fresh and saline ice is not considerable (Notz, 2005). The details of saline ice growth are given in Appendix B.

Such a simple analytical model, which ignores time delay in thermal diffusion, can give errors when the air temperature is quickly moving towards water freezing point, and the microporosity change in nature is slowed by thermal inertia. This error can be eliminated only by solving diffusion equations for snow and saline ice layers assuming external convection from the air. The difference between analytical and numerical predictions will be presented in the results of this study.

2.3. Analytical 1-D resistive ridge model

Ridge consolidation has many similarities with level ice growth, but there are some vital differences: a) the ridge keel is porous with a macroporosity η_m while the level ice grows from liquid and b) the spatially inhomogeneous top and bottom surfaces. The macroporosity may be adjusted by modifying the latent heat so that it becomes (Leppäranta and Hakala, 1992):

$$L_r = \eta_m L_i \tag{12}$$

This assumption is valid for homogeneous ridges with small voids so that the vertical temperature gradient is constant horizontally. In a natural real ridge, the voids are so large that the vertical temperature profiles may vary horizontally. This makes horizontal heat fluxes occur inside ice ridges (Leppäranta et al., 1995), and the ice-water interface has an ellipse shape where new ice is forming (Petrich et al., 2007). These inhomogeneities caused by the relatively large voids/consolidated layer thickness ratios are more complicated to handle in our analytical one-dimensional models. In our simplified sketch of an ice ridge (Fig. 2b) its macroporosity is defined as $w_v/(w_v + w)$.

Let us start with the top surface, or the sail, characterized by its height s. It gives a locally changing ratio of thermal resistances and the total area via which heat is extracted to the air. But ridge sails also

change the distribution of snow, creating accumulations and snow-free surfaces. It is making top surface conduction to be a 2D or even 3D problem in contrast to level ice. These factors are changing thermal resistance of ridge sail and its top surface temperature, making the analysis of field data much more complicated due to the difference in temperatures of different parts of the consolidated layer. The top surface in natural ridges can be colder while the sail temperature at the water level can be warmer than in sail free consolidated layer (Leppäranta et al., 1995).

In this model, we assume that snow thickness is the same on the top and on the sides of ice ridge blocks. It is important to mention that when snow is thick enough and its top surface is even, other models to handle sail thermodynamics might be used. Snow may accumulate in different ways on and around a ridge sail and the choice of the model requires detailed investigations of snow thickness spatial distribution.

Thermodynamics of ridge sail, not covered by a thick layer of snow, is mainly affected by two factors: additional thermal resistance from the thicker ice layer, which should decrease heat flux below water level, and additional air-snow or air-ice interface area, which should increase heat flux below water level. Both factors should be considered to predict heat flux and temperature profile in ice ridge. For example, an initial thickness equal to the sail height can decrease vertical heat flux during the starting period of consolidation.

We have applied the theory of extended surfaces (Incropera et al., 2013). Fin performance defines an effective heat flux q_f and a corresponding thermal resistance R_f through the snow-covered sail (Fig. 2c), and it assumes a spatially constant base temperature T_{base}. The theory compares the effective heat flux through the fin q_f with that of a flat surface of the same top area A_c and defines a fin performance ϵ_f:

$$\epsilon_f = \frac{q_f}{HA_c(T_{base} - T_a)} \tag{13}$$

where H is the combined heat transfer coefficient of air and snow, $A_c = wl$ is the fin cross-section area, w is the fin thickness, l is the fin length, and T_{base} is the fin base temperature.

The thermal resistance of the snow-covered sail becomes

$$R_f = (T_{base} - T_a)A_c/q_f \tag{14}$$

The vertical heat flux through the sail and the snow q_f gives information about the total thermal resistance of the system consisting out of ice, snow, and air above the consolidated layer. Fin performance ϵ_f can tell how much presence of sail increase or decrease the consolidation rate.

When ice is snow-free, the thermal resistance of air is equal to the turbulence resistance $1/H_{ia}$. When there is snow on the top of the ice, the heat transfer coefficient H can be estimated as:

$$H = \left(\frac{1}{H_{ia}} + \frac{h_s}{k_s}\right)^{-1} \tag{15}$$

The bottom surface is also inhomogeneous and here we simply define two different vertical one-dimensional heat fluxes, up from a void (Fig. 2a) and through a block (Fig. 2c). The model assumes that sail exists only on top of blocks and the heat flux up from a ridge void q_v can be found as:

$$q_v = \frac{T_f - T_a}{R_a + R_s + R_c} \tag{16}$$

$$R_c = h_c/k_i \tag{17}$$

where R_c is the thermal resistance of the consolidated layer.

The heat flux in the ridge block q_b with sail can be found as:

$$q_b = \frac{T_f - T_a}{R_f + R_c + 0.5 \cdot R_b} \tag{18}$$

where R_f is the thermal resistance of finned surface (a sail), R_b is the rubble block thermal resistance that can be expressed as:

$$R_b = \frac{w}{4k_i}\left(\frac{\pi}{2} - 1\right) \tag{19}$$

This additional thermal resistance is changing the temperature at the bottom level of the consolidated layer, making blocks colder than water freezing point.

The effective, or total heat flux in the ridge is equal to the latent flux from consolidation:

$$q_r = q_v\eta_t + q_b(1 - \eta_m) = \rho_i L_r \frac{dh_c}{dt} \tag{20}$$

The estimation of ice thickness from temperature profile usually requires several assumptions. It is a common practice to assume that temperature profile in solid ice is linear below the upper layer of approximately 20 cm, where the temperatures depend on daily air temperature variations (Leppäranta et al., 1995). The difference in temperature profiles between ridge voids and blocks is making experimental thickness estimation from the measured temperature profile more complicated, as well as analysis of experimental heat fluxes due to ridge inhomogeneity.

2.4. Numerical model of level ice and ridge

The numerical simulations of level ice and ridge consolidation were performed with finite element analysis simulation software COMSOL Multiphysics 5.3a using the front tracking method. The position of the ice-water boundary was defined by Stefan's energy balance condition (Eq. (22), where the difference of heat fluxes in two materials is equal to the amount of new solid formed or melted.

This numerical model requires the following material parameters for ice and water: thermal conductivity, heat capacity, density, coefficient of thermal expansion, latent heat of fusion and water kinematic viscosity. Saline ice thermodynamic parameter values are described in Appendix B. Other values were obtained using the Gibbs SeaWater Oceanographic Toolbox of TEOS-10 (Millero, 2010). Thermal boundary conditions were defined as thermal insulation at the sides and at the liquid bottom (Fig. 2b). The air-ice interface has a temperature-dependent incoming heat flux based on either convective model with a constant heat transfer coefficient H_{ia} or on radiative heat balance for both level ice and the ridge.

The heat flux balance at the air-snow interface for the convective model is described as follows:

$$H_{ia}(T_a - T_{as}) = k_s\left(\frac{\partial^2 T_s}{\partial x^2} + \frac{\partial^2 T_s}{\partial z^2}\right) \tag{21}$$

The top surface heat flux balance for the radiative numerical model is described in Eq. (3). The heat flux balance at the ice-water interface is

$$\rho_i L_i v_n = k_i \frac{\partial T_i}{\partial n} - q_w \tag{22}$$

where v_n is the normal velocity of the ice-water interface, $\partial T_i/\partial n$ is the normal derivative of the ice temperature at the interface, and q_w is the heat flux from the water.

Heat diffusion within the snow and ice is described by

$$\rho_{s,i}c_{s,i}\frac{\partial T_{s,i}}{\partial t} = k_{s,i}\left(\frac{\partial^2 T_{s,i}}{\partial x^2} + \frac{\partial^2 T_{s,i}}{\partial z^2}\right) \tag{23}$$

The numerical model includes a thin initial ice thickness h_0 of 5 cm at the air-water interface. In numerical modelling, we used an average snow density value of 374 kg/m^3, obtained from measurements taken during the winter end on Svalbard (Sand et al., 2003) and the thermal conductivity value of 0.21 W/m^2 obtained from the temperature measurements analysis using Eq. (9).
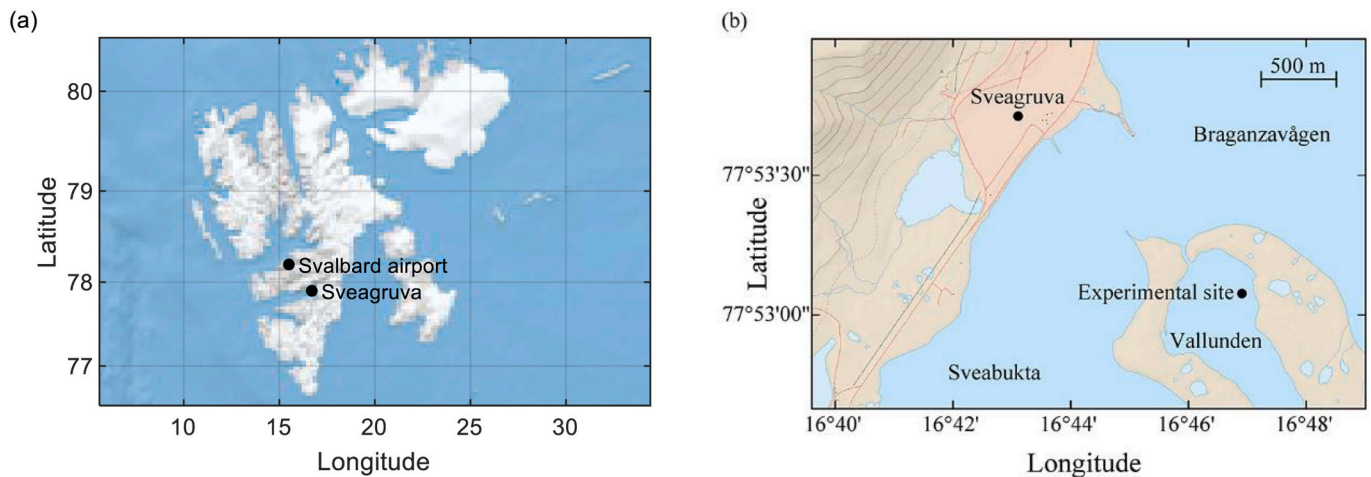
Fig. 3. Location of weather stations in Svalbard (a) and location of the experimental site in Van Mijenfjorden (b) on the map by Norwegian Polar Institute.
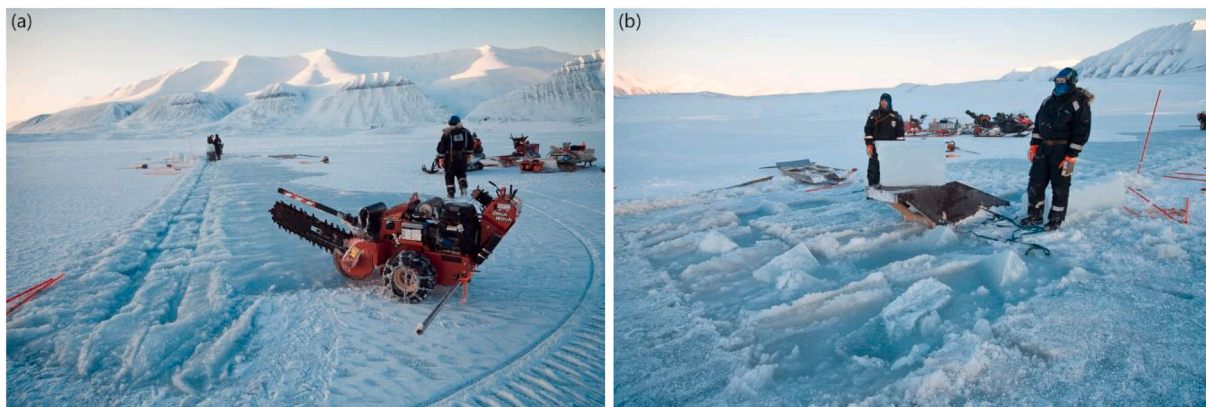

Fig. 4. Feeding channel (a) and ridge building using the ramp (b).

3. Field measurements

3.1. Methods and preparations

The field experiment in the consolidation of artificial ice ridge was performed during 66 days from 25 February 2017 until 2 May 2017 in seawater Vallunden lagoon in the Van Mijenfjorden in Svalbard (Fig. 3).

The ridge was made of 55 blocks from 50 cm thick ice, totally 11.4 m^3 of ice. The average initial level ice salinity was 3.8 ppt and the average initial block temperature was −7.8 °C. A basin 3.0 m by 4.9 m was made in the level ice cover, and the blocks were dumped into the basin. The ice blocks were cut in the feeding channel using a trencher. After that, the blocks were placed into the water basin using rope, ramp, and snowmobile (Fig. 4).

The following information was collected during 4 visits: temperature, salinity, and density profiles. We collected 3 vertical cores during the visit 1 and 12 vertical cores at visit 4 to investigate ridge morphology. The value of initial macroporosity was estimated based on the volume of ice blocks measured during visit 1 and final ridge volume measured during visit 4. The initial volume of ice was calculated using measured dimensions of all 55 blocks that were used for the ridge creation. The final volume of ice was estimated using keel depth values from 12 cores drilled during visit 4.

Both level ice and ridge were instrumented with thermistor strings. We used two strings from GeoPrecision GmbH with Dallas DS1820 temperature sensors. The accuracy of sensors was 0.25 °C, the resolution was 0.065 °C, the sampling time was 10 min. In the ridge, the thermistor was in the sail with 15 cm freeboard and logged continuously until May 4. Level ice had 7 cm freeboard and its temperature profile was logged until March 18. The snow was kept above the level ice near the thermistor location.

Three cores were used to measure initial parameters of level ice from which the ridge was formed during visit 1. One core of the level ice and of the ridge were used for salinity and density profiles at visit 4. The vertical resolution of salinity and density profiles was 5 cm.

During all 4 visits of the experimental site from 25 February 2017 until 4 May 2017 following parameters were measured for level ice and model ridge: ice and snow thickness, ice salinity and density vertical profiles.

Model input data includes two main groups of parameters: atmospheric data from weather stations or remote sensors, and physical parameters of ice and snow. Sea ice thermodynamic parameters including heat capacity, thermal conductivity, latent heat and solid fraction were calculated from Notz (2005). Data from weather stations in Svalbard were collected using web services yr.no and eklima.no provided by the Norwegian Meteorological Institute. Most information for the top surface heat balance was received from the closest weather station 99760 Sveagruva, located 2 km from the experimental site. Sveagruva weather station is providing information about air temperature, humidity and wind speed. Cloudiness data was received from 99840 Svalbard airport weather station in 40 km from the experimental site. The number of clear and overcast days at Sveagruva and Svalbard airport weather stations was similar from the 1970s until the 1990s (Førland et al., 1997). Local cloudiness at the experimental site was received from the
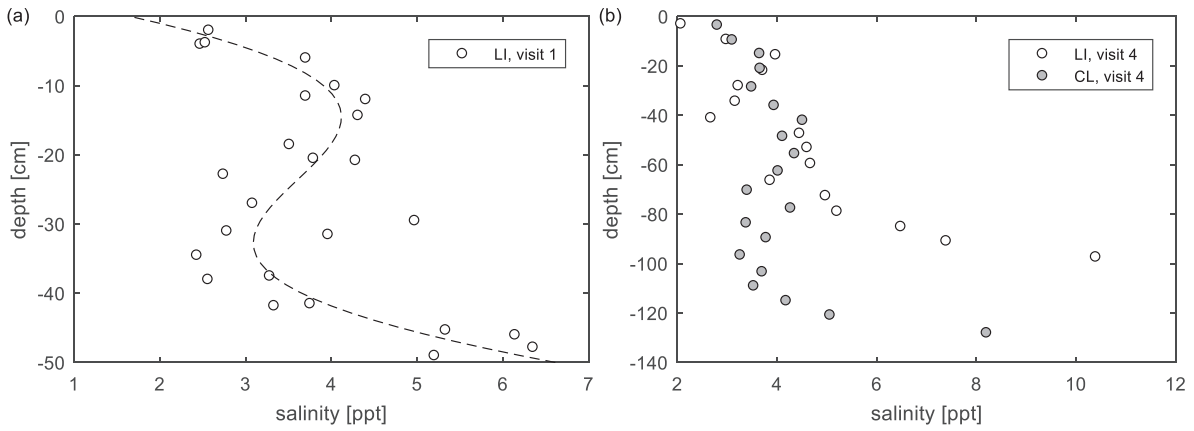
Fig. 5. Salinity profiles of the level ice for visit 1 (a) and of the level ice and the consolidated layer for visit 4 (b). Dashed line represents curve fitting of salinity values to a sum of sinusoidal functions.
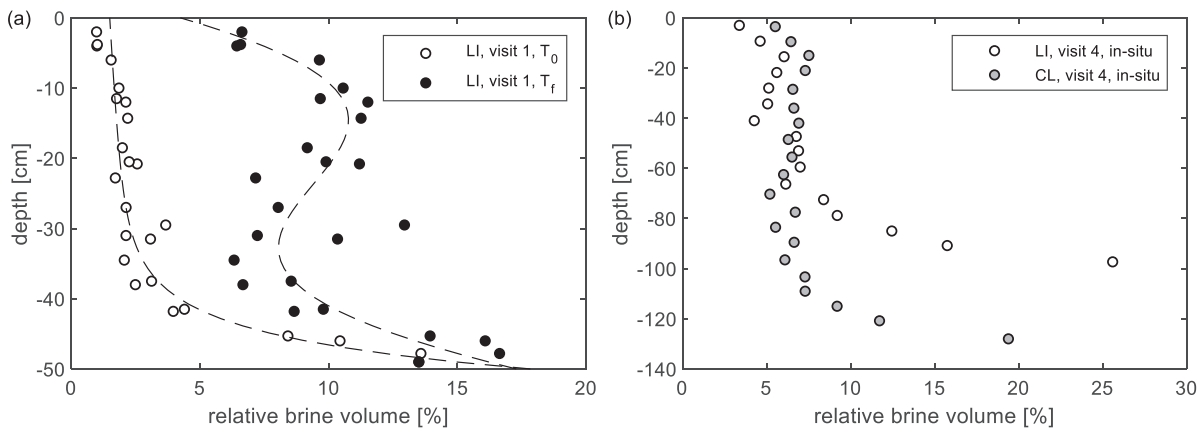

Fig. 6. Relative brine volume profile estimated for the level ice in-situ temperature T_0 and for the water freezing temperature T_f for visit 1 (a) and for in-situ temperatures of the level and the consolidated layer and visit 4 (b) based on the measured values of ice salinity and density. Dashed lines represent curve fitting of brine volume to a sum of sinusoidal functions.

Icosahedral Nonhydrostatic (ICON) Modelling Framework from the German Weather Service. Coefficients for sensible and latent heat fluxes were found from Smith (1988).

Ice thickness estimation from temperature profile was based on the temperature data below the upper 20 cm, where values are not sensible to daily air temperature variations. All the sensors with temperature values lower than water freezing temperature T_f by more than a chosen threshold ΔT of 1 °C were considered frozen, and the highest and lowest measurement points were used for linear extrapolation of temperature profile to obtain ice thickness value. The sensitivity of this method to the chosen threshold will be described in the paper results.
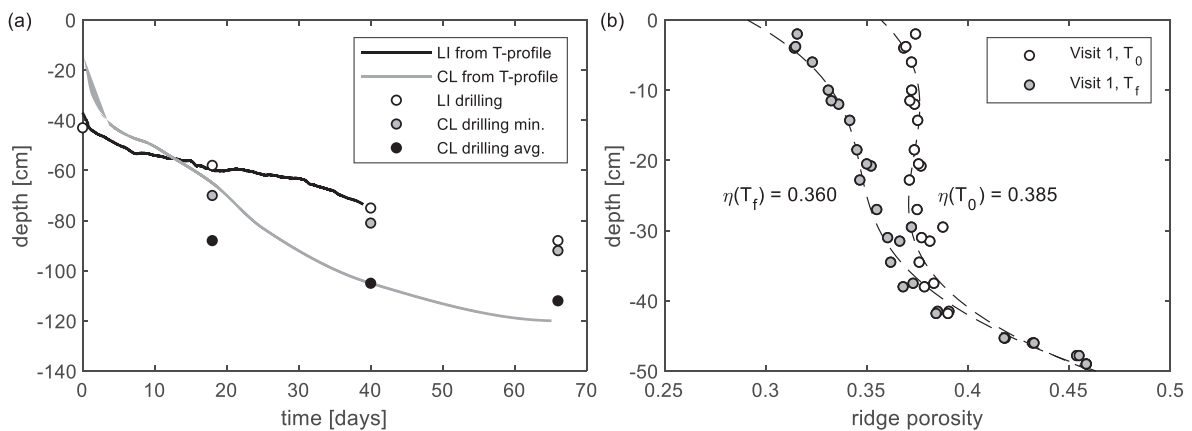

Fig. 7. Ice draft development of level ice and consolidated layer (a) and the ridge total porosity η profile for visit 1 for the level ice in-situ temperature T_0 and water freezing temperature T_f (b). The estimation of the ridge total porosity assumes that the ridge initial salinity and gas volume are identical to ones measured for the level ice. Dashed lines represent curve fitting of porosity values to a sum of sinusoidal functions.

3.2. Measurements

In the following sections we will describe input data and results of our thermodynamic models' application. Input data includes two main group of parameters: atmospheric data from weather stations or remote sensors, and physical parameters of ice and snow. The average cloudiness c measured at Svalbard airport weather station near Longyearbyen was 0.63 during the experimental time. The Icosahedral Nonhydrostatic (ICON) Modelling Framework from German Weather Service showed the average cloud cover of 0.57 for Longyearbyen airport and 0.58 for Sveagruva.

The air temperature at the Sveagruva weather station was measured hourly and was in the range from −28.5 °C to 3.0 °C with the average value of −12.6 °C, which was only 0.3 °C warmer than the historical value for March and April (Førland et al., 1997). The relative humidity RH during the experiment was in the range from 0.44 to 0.95 with the average value of 0.75 for both Sveagruva and Longyearbyen, 0.06 lower than the historical average. The average wind speed at Sveagruva during our experiment was 4.7 m/s.

Sea ice thermodynamic parameters depend on its salinity. Cores drilled from level ice and model ridge during visit 1 and visit 4 were used to obtained salinity profiles (Fig. 5). Comparing level ice salinity profiles, it can be argued that about 4 cm of ice formed above the initial top surface between two visits. The level ice salinity after 66 days changed from 3.8 ppt to 4.6 ppt, consolidated layer final salinity was 4.1 ppt.

Relative brine and gas volumes were estimated using in-situ measurements of ice temperature, salinity, and density using Cox and Weeks (1983). Values of the estimated relative brine volume are presented for level ice at visit 1 for its in-situ temperature T_0 and for the measured water freezing temperature T_f (Fig. 6a) and for both level ice and consolidated layer at their in-situ temperatures during visit 4 (Fig. 6b). We assumed that the rubble blocks have a uniform temperature of the water freezing point T_f after the end of the initial phase of the ridge consolidation. We also assumed that the initial salinity of rubble blocks is equal to the measured salinity of the level ice during visit 1. The brine
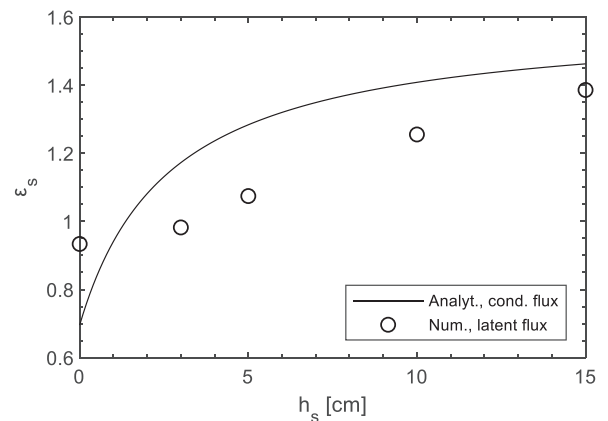
Table 1
Evolution of the main level ice and consolidated layer parameters.

Parameter	Visit			
	1	2	3	4
Number of LI/CL cores	3/0	0/2	0/4	1/12
Min. CL thickness [m]	0.00	0.78	0.97	1.00
Avg. CL thickness [m]	–	0.96	1.13	1.20
LI thickness [m]	0.50	0.65	0.82	0.99
CL snow thickness [m]	0.00	0.13	0.07	0.09
LI snow thickness [m]	0.02	0.11	0.02	0.05
CL salinity [ppt]	3.8	4.2	3.8	4.1
LI salinity [ppt]	3.8	–	–	4.6
FDD [°d]	705	915	1228	1421
Ridge macroporosity	0.36	–	–	0.00

Fig. 9. Sail performance ϵ_s vs snow thickness h_s for 15 cm sail height and 50 cm sail width from the analytical sail model and its effect on consolidated layer thickness from the numerical convective model.
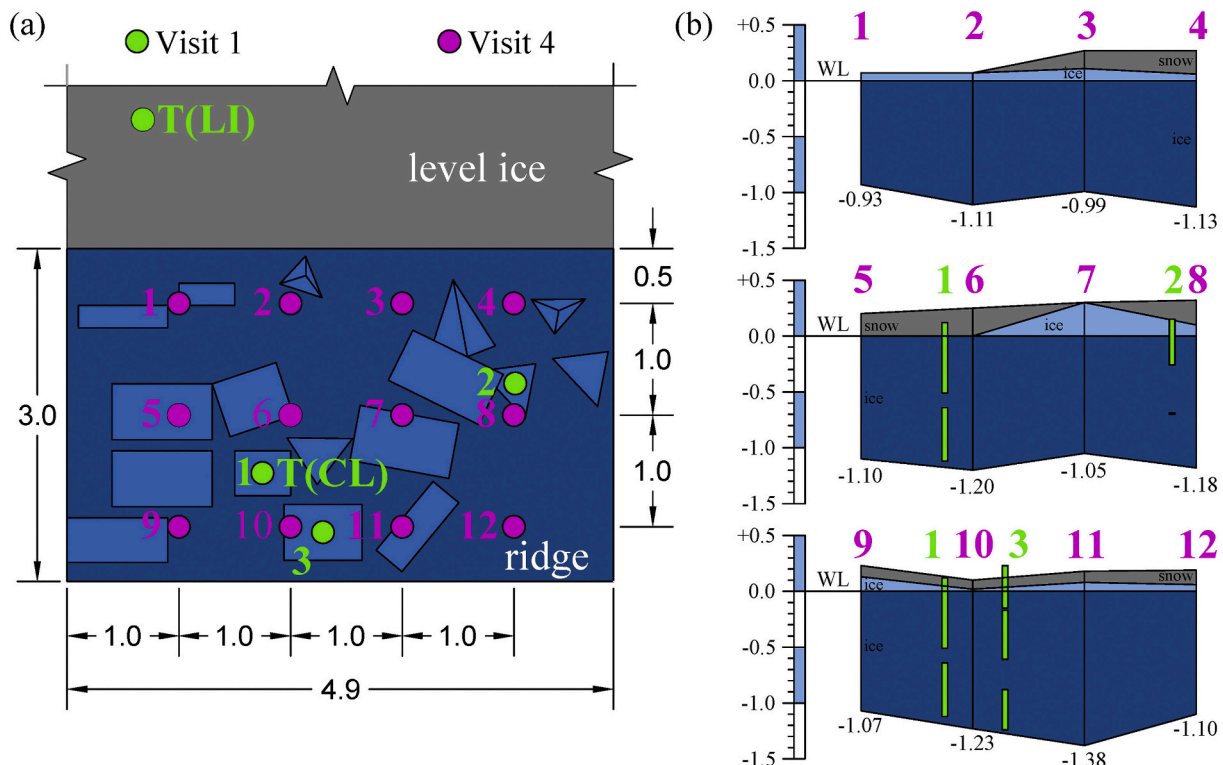
Fig. 8. Ridge top plan (a) and three vertical profiles (b) during visit 1 and 4. All sizes are given in meters.

volume values of the rubble was assumed to be equal to the brine volume of the level ice estimated for the water freezing temperature T_f using Cox and Weeks (1983).

Level ice grew from 50 cm to 99 cm, while the consolidated layer grew from 0 until 120 ± 12 cm. The average freeboard after the experiments was 7 cm for level ice and 8 cm for the consolidated layer. The temporal development of level ice and consolidated layer draft is presented in Fig. 7a: from the drilling during 4 visits and from the vertical temperature profiles measured by thermistors. During visit 4 salinity, density and temperature of level ice and consolidated layer were measured, giving 8% of liquid volume fraction (Fig. 6b) and 2% of gas volume fraction.

Snow thickness above the level ice varied in the range 2–11 cm, while snow thickness above the ridge was 0–13 cm. For measured snow thickness and estimated snow thermal conductivity at the ridge, the heat transfer coefficient H of air and snow varied in the range 1.4–21 W/m²K. The summary of the measured parameters during each visit is presented in Table 1.

Initial ridge total porosity η was estimated for the measured level ice in-situ temperature, density, and salinity combined with the measured initial macroporosity. It was assumed that the salinity and gas volume, measured for the level ice during visit 1, would remain unchanged during the initial stage of the ridge consolidation. The value $\eta(T_0)$ indicates the total porosity of the ridge before the block temperature started to change from the initial temperature T_0 to the seawater freezing temperature T_f. The value of the ridge total porosity after the initial phase of consolidation $\eta(T_f)$ was estimated assuming that the sensible heat of the cold blocks at the temperature T_0 was conserved and transferred into the new ice formation. During the initial phase, the brine volume of ice blocks increased as shown in Fig. 6a. The change of the total porosity during the initial phase corresponding to the change of block temperature from T_0 to T_f is shown in Fig. 7b using the vertical salinity, density, and temperature profile of each block forming the ridge. Due to the block average initial temperature $\overline{T_0}$ of -7.8 °C, the ridge total porosity should decrease from 0.39 to 0.36. The ridge initial macroporosity was found from the ridge initial and final volumes. The initial ridge volume was estimated based on the measured volume of ice blocks, while the final ridge volume was estimated from its morphology at visit 4 (Fig. 8).

4. Results

Before the analysis of the provided fieldwork experiment, we will present more general results of our analytical and numerical investigations, where we will try to improve understanding of ridge thermodynamics and validation methods for ridge models. We will focus on thermodynamic effects from the main differences between level ice

and ice ridge including ridge sail, snow on its top, ridge rubble, and ridge inhomogeneity (Section 4.1). After that, we will describe details of the consolidation experiment and how general conclusions can help with its analysis and model validation (Sections 4.2–4.5).

4.1. Sail and rubble effects

The presence of the sail has two different effects, its thickness provides additional insulation and delays consolidation while the irregular surface gives a higher exposed area and enhances the consolidation. The snow cover is a key factor here as it strongly affects the heat transfer coefficient H from Eq. (15) and with this the sail effect. Below we will examine how the snow cover affects the analytical solution of the surface flux (by the fin performance ϵ_s in Eq. (13) and further, apply the two-dimensional numerical solution (Section 2.4). The solution for the fin performance shows that it increases with increasing snow thickness, and for snow thicknesses above 1 cm it predicts that the presence of a sail increases the heat flux compared to the same snow cover of flat ice (Fig. 9). This solution (Appendix C) assumes that the temperature below the sail T_{base} (base temperature) is not affected by the surface conditions and this is not strictly true. Numerical simulations confirm the general trend of increasing the effect of thicker snow but modifies the effect for thin snow covers.

Defining lower boundary of the consolidated layer in the ridge is also complicated by its inhomogeneity. In our consideration, the thickness of the consolidated layer is defined by newly formed ice in the void (Fig. 2b). In the void the consolidated layer thickness similarly to the level ice thickness can be estimated from temperature profiles as the ice temperature is always less than equal to T_f, and the water below is always warmer or equal to T_f similar (Fig. 2a). In the block, the boundary of the consolidated layer is somewhere inside the block (Fig. 2c) and the temperature profile cannot be used the same way as above to define the thickness of the consolidated layer. The spatial resolution of temperature measurements combined with the non-linear temperature profile close to the bottom of the block and the daily variations in the top makes it necessary to extrapolate. A linear section of temperature profile for extrapolation was chosen by cutting off upper nodes affected by daily temperature changes and bottom nodes in the non-linear part. We cut off nodes in the upper 20 cm of the profile below the snow-ice interface and nodes in the bottom part of the profile where the temperature is higher or equal to $T_f - \Delta T$. Threshold ΔT can be set for example 1 °C or 0.5 °C. Further, a linear temperature profile is extrapolated to T_f, and the thickness of the consolidated layer in the block is defined.

Fig. 10 shows temperature profiles through the void and block at two different time moments of our numerical simulation. Defined according to the description above, the boundary of the consolidated layer in a void and a block are shown on the plots. The figure illustrates that there
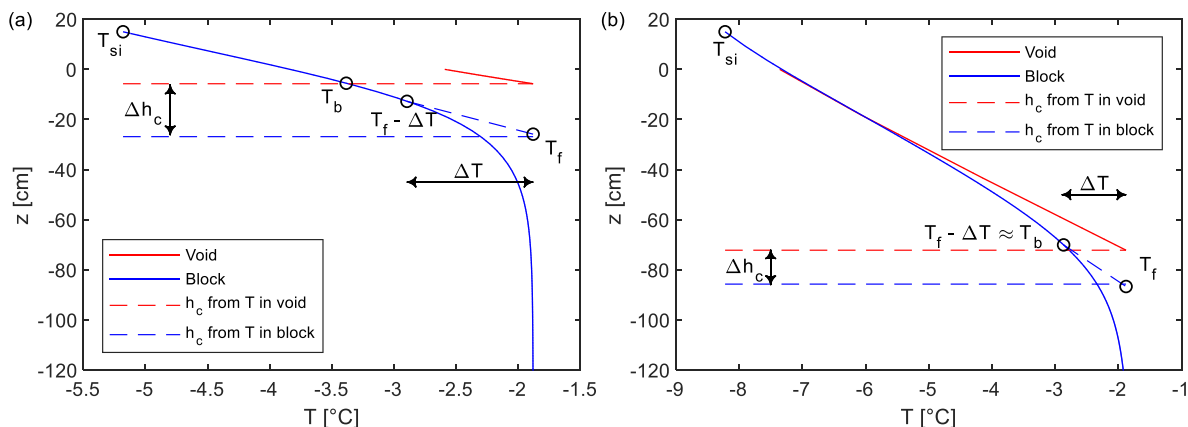

Fig. 10. Temperature profiles in ridge void and block after 1 day (a) and after 25 days (b) of consolidation from the numerical model.
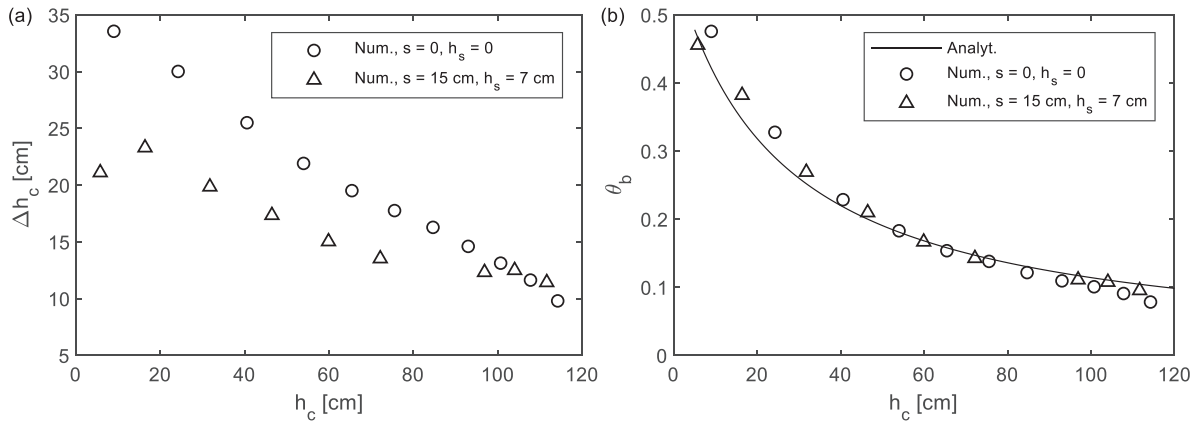
Fig. 11. Thickness overestimation Δh_c based on temperature profiles from numerical modelling using $\Delta T = 1\,^\circ C$ (a) and block bottom dimensionless temperature θ_b based on analytical and numerical models (b).

may be significant differences in the estimated thicknesses of the consolidated layer (Δh_c up to 0.2 m) for the chosen threshold ΔT of 1 °C. Considering our minimum definition of the consolidated layer (Fig. 1), which corresponds with the one derived from a void, we call the difference in estimated thicknesses as an overestimation.

Numerical simulations of this overestimation were done without sail and snow, and with 15 cm high sail and 7 cm thick snow to check how temperature profiles are affected by snow and sail. The ice thickness overestimation decreased with increasing consolidated layer thickness and depended on sail and snow (Fig. 11a). It also depended on the ice temperature (not shown in the figure). A dimensionless block temperature θ_b can be defined as:

$$\theta_b = \frac{T_b - T_f}{T_{si} - T_f} = \frac{\Delta T_b}{\Delta T_c + \Delta T_b} \qquad (24)$$

where T_b is the temperature at the center of the block at the bottom level of the consolidated layer with a minimum thickness (Fig. 10a).

The thickness overestimation Δh_c depends on the block temperature T_b (Fig. 10a) as:

$$\frac{\Delta h_c}{h_c}(\Delta T = \Delta T_b) = \theta_b \qquad (25)$$

From the resistive analytical model described in Section 2.3, the dimensionless block temperature θ_b is defined by the block thickness w, and the consolidated layer thickness h_c as:

$$\theta_b = \frac{R_b}{R_c + R_b} = \left(1 + \frac{7h_c}{w}\right)^{-1} \qquad (26)$$

The condition $\Delta T = \Delta T_b$ is complicated to use for the thickness estimation in experiments because it requires knowledge of the consolidated layer thickness. For the smaller thresholds $\Delta T < \Delta T_b$ the values of the thickness overestimation are larger and cannot be described by the resistive model. The larger thresholds $\Delta T > \Delta T_b$ correspond with smaller overestimations but can dramatically increase errors of the temperature profile extrapolation, especially for the initial phase of the consolidation. Thus, it is recommended to use threshold range close to the ΔT_b for the later stages of the consolidation. For our experiments ΔT_b lays in the range between $(T_f - T_{si})/5$ and $(T_f - T_{si})/10$ during the most of the time (Fig. 11b).

In comparison to thickness measurements, which are representing average heat transfer over ridge void and surrounding blocks, temperature profile measurements are representing only local vertical heat transfer. As can be seen from Fig. 10, large-scale ridges are inhomogeneous and vertical temperature gradient can be significantly different for different parts of a ridge. It can be important for the validation of an analytical consolidati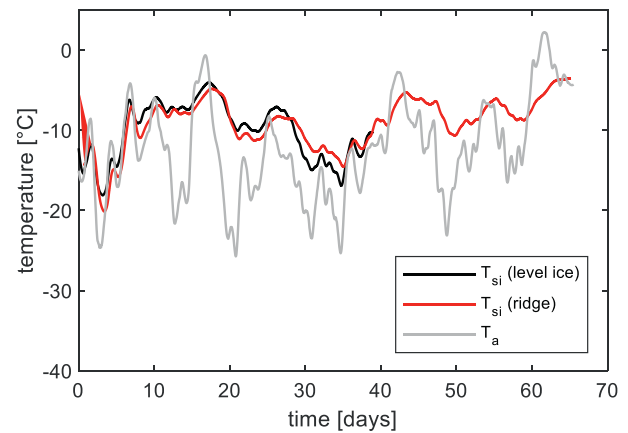on model because almost any analytical model is only able to describe average heat flow through different parts or the whole ice ridge.

Fig. 12. Snow-ice interface temperature T_{si} and air ambient temperature T_a development for level ice and the ridge.

4.2. Top surface heat balance

The air and snow-ice interface temperature of level ice and the ridge are shown in Fig. 12. The ridge top surface was colder than of level ice during the first 20 days of our experiment. The thermal resistance of air was much smaller than thermal resistances of both ice and snow: the average air temperature was only 0.3 °C lower than the measured top surface temperature of snow, while the average difference between the top and bottom surface temperatures was 8.3 °C for ice and 4.1 °C for snow.

Let us proceed with examining how the analytical models (Section 2.3) with the two different atmospheric fluxes (simple convective or more advanced radiative) predict the air-snow temperature T_{as}. We assume that the air temperature was known and define a temperature difference over the air boundary layer $\Delta T_a = T_{as} - T_a$. The radiative model is more complicated and to estimate its sensitivity, the uncertainty of the three following aspects were examined:

- Longwave radiation model: Maykut (1986), Rosati and Miyakoda (1988).
- Cloudiness: from the weather station in Longyearbyen, from the ICON model for Svea.
- Turbulent heat transfer coefficient: Smith (1988), Rosati and Miyakoda (1988).
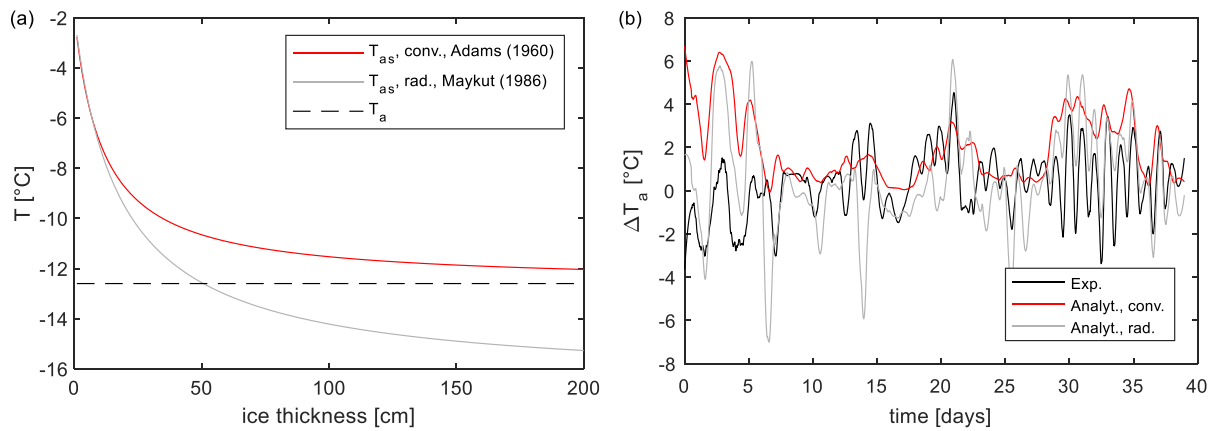
Fig. 13. Surface temperature T_{as} vs ice thickness h_i for the average experimental meteorological conditions (a) and the difference between the top surface and air temperatures ΔT_a from the level ice experiment, radiative and convective analytical models based on experimentally measured conductive heat flux q_c and meteorological data (b).
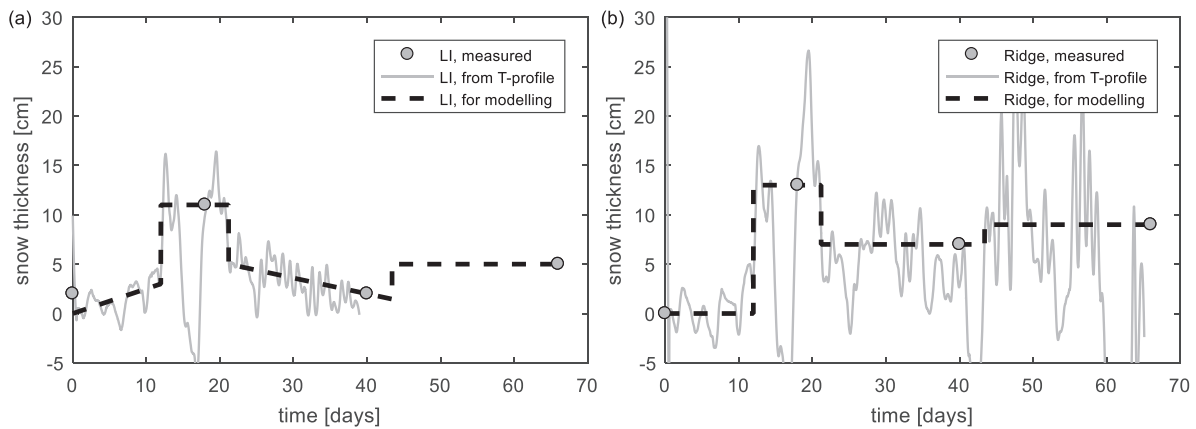

Fig. 14. Snow thickness above level ice (a) and consolidated layer (b) vs time.

The analytical dependence of the air-snow temperature on the ice thickness for the average experimental meteorological conditions is given in Fig. 13a and shows that the convective model predicts a warmer snow surface. The convective model does, by definition, predict a snow or ice top surface temperature T_{as} warmer than the air temperature T_a (if T_a is colder than water). In nature, the snow surface can be colder than the air temperature (Fig. 13b) and this is known as ground inversion. This phenomenon can only be predicted by the radiative model. Fig. 13b shows ΔT_a derived directly from the level ice measurements and for the two models based on meteorological data and experimentally measured conductive heat flux q_c and not including snow parameters using Eqs. (3) and (5).

The turbulent heat transfer coefficient has relatively little effect of 2% of the heat flux. Averaged over time difference between analytical and experimental values of ΔT_a was in the range of $-2.5\dots0.6$ °C for different parametrisation giving the best fit for the models of Maykut (1986), Smith (1988), and cloudiness data from the Longyearbyen weather station. A simple convective model by Adams et al. (1960) gave a difference of 1.7 °C (Fig. 13b).

As a conclusion, it can be said that while radiative models can predict top surface temperatures more accurately, an error of the convective model is small enough considering its simplicity and applicability for resistive thermodynamic models.

4.3. Snow conditions

Snow thickness between visits was estimated using Eq. (9). In the

first approach snow thermal conductivity value was chosen arbitrarily. From the values of snow thickness, time moments of snow thickness transition were found. Snow thickness values were linearly interpolated to fit the shape of estimated values and measured snow thickness values. After that thermal conductivity values were estimated based on assumed snow thickness in time. The final value of snow thermal conductivity was obtained using statistical analysis of estimated values, based on conductive heat flux balance in snow and ice.

The snow layer has thermal resistance comparable with ice; also, it is a material with high uncertainties in its thermodynamic characteristics. Snow thickness was measured directly only during four visits. The snow thermal conductivity value of 0.21 W/m² was obtained based on the level ice temperature profile and four in-situ measurements of snow thickness, requested the fit of thermal resistance values Eq. (9). Further, the reverse task can be solved. Assuming a constant snow thermal conductivity and knowing ice temperature profile, snow thickness in time during the experiment was estimated (Fig. 14) and further used in numerical modelling. Both for level ice and model ridge snow thickness was considerably low except days 12–21.

The analysis of snow thickness effects on heat transfer in the ridge is more complicated than for pure one-dimensional level ice. The temperature profile in ridge blocks is non-linear even under steady-state ambient conditions: temperature gradient is slightly lower in sail (Eq. (49) and is also decreasing towards the block bottom. With our measured snow thickness and estimated snow thermal conductivity, the heat transfer coefficient H varied in the range 1.4–21 W/m²K according to Eq. (15).
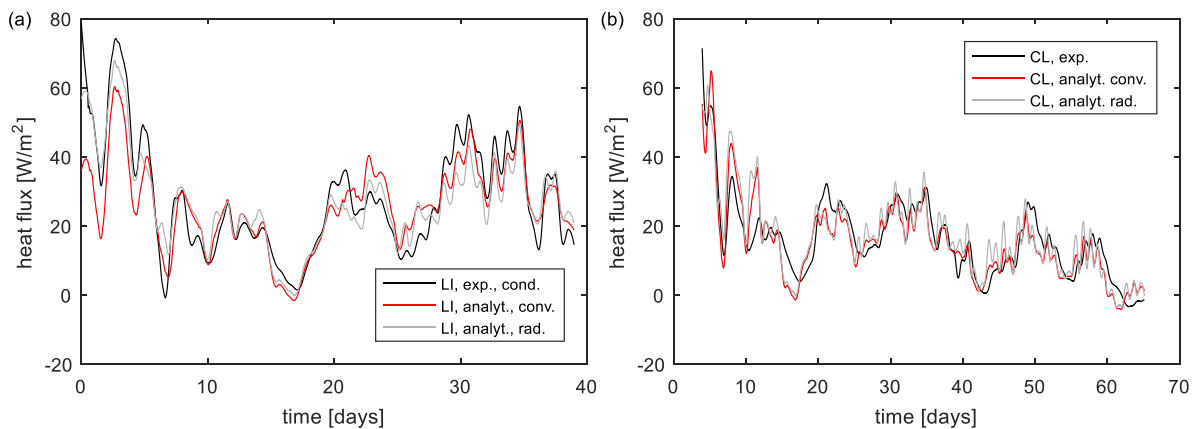
Fig. 15. Vertical heat fluxes from experiment, convective and radiative analytical models in level ice (a) and in the ridge (b).

Table 2
Ice thickness and mean vertical heat flux values after visit 4 (visit 3).

Ice type	Model	s [m]	h analyt. [m]	h num. [m]	h exp. [m]	q analyt. [W/m^2]	q num. [W/m^2]	q exp. [W/m^2]
LI	Conv.	0	0.95	0.94	0.95	20.3 (25.9)	19.9 (27.0)	(27.9)
	Rad.	0	1.02	0.95		21.2 (27.0)	20.9 (28.3)	
CL	Conv.	0	1.13	1.14	1.20	20.3	20.3	19.0
	Rad.	0	1.23	1.20		21.6	21.0	
	Conv.	0.15	1.21	1.16		21.4	19.4	
	Rad.	0.15	–	1.23		–	22.2	

4.4. Vertical heat fluxes

In two previous sections we estimated the main parameters of air and snow models fitting our field observations. It is of interest to see how these models can predict heat fluxes found experimentally from ice temperature, density, and salinity vertical profiles. Analytically and numerically estimated heat fluxes are only based on meteorological data and measured or estimated ice and snow thermodynamic parameters. The average level ice heat flux from analytical convective and radiative models are 7% and 3% lower than from the experiment (Fig. 15a).

Modelling and validation of heat fluxes for ridges are much more complicated due to its inhomogeneity and corresponding different boundary conditions at different vertical profiles. Fig. 15b shows the results of the simplest "flat" analytical models of ridge consolidation. In that model there is no sail. Our experimental temperature profile was measured in the ridge block. Experimental values from the first 4 days are not presented because not enough sensors were frozen for heat flux estimation. The "flat" analytical radiative model gives 6% higher flux than experimentally estimated, the convective model gives 5% lower flux for days 5–66 of our experiment.

There is a difference between average fluxes in voids and blocks. In our numerical radiative model heat flux in the void was 22.6 W/m^2, while average flux in the block was 19.3 W/m^2, significantly closer to the experimental heat flux of 19.0 W/m^2. As it was described in the sail effect section, the largest heat flux increase is only observed in the vicinity of sail walls, while heat fluxes in the middle of block and void are almost equal.

As a summary, our analytical and numerical models are predicting heat fluxes equally accurate for level ice and ridges, while the more advanced radiative model is performing slightly better than convective (Table 2).

4.5. Ice thickness

Level ice thickness from direct measurements at visit 4 was 99 cm including 4 cm of top surface growth. Our convective and radiative
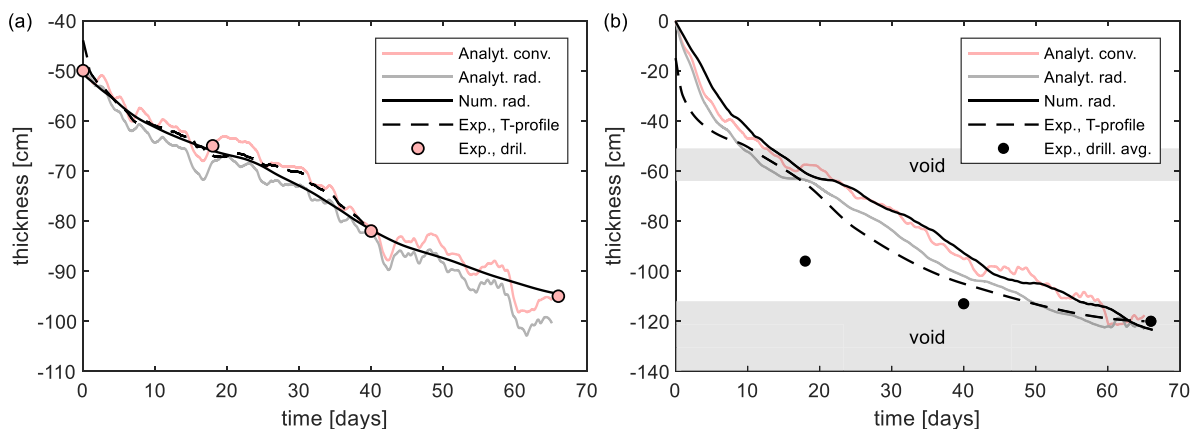

Fig. 16. Level ice (a) and consolidated layer (b) thickness vs time from the experiment, analytical and numerical models. The grey shaded area corresponds to the voids found from the ridge drilling during visit 1.
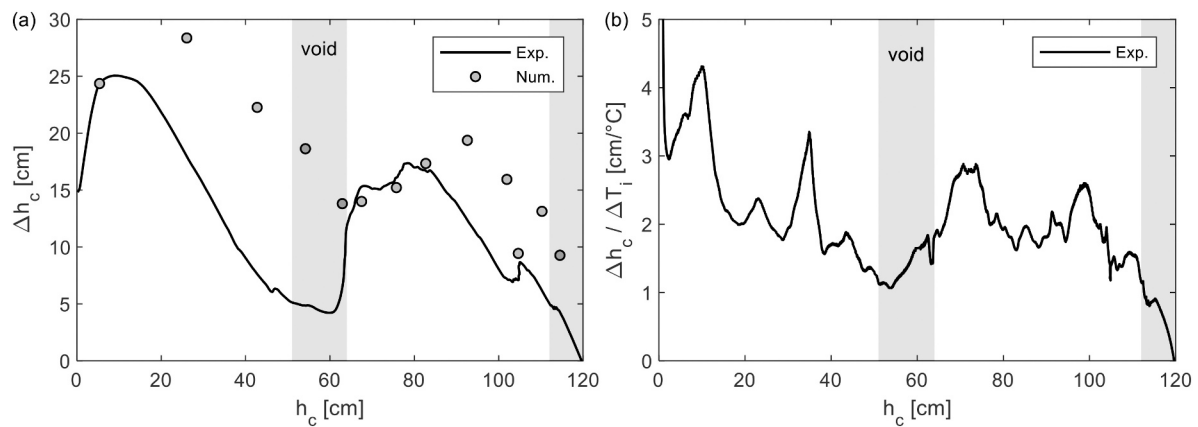
Fig. 17. Total thickness overestimation Δh_c (a) and its values per temperature difference in ice $\Delta T_i = T_f - T_{si}$ (b) vs consolidated layer thickness. The grey shaded area corresponds to the voids found from the ridge drilling during visit 1.

analytical models predicted the thickness of 95 cm and 102 cm correspondingly (Fig. 16a), while numerical models gave 94–95 cm. The measured consolidated layer thickness was 120 cm, while convective and radiative analytical models gave 113 cm and 123 cm (Fig. 16b). The numerical model predicted a slightly lower thickness due to considering thermal inertia and ridge initial phase. For both level ice and consolidated layer, the numerical radiative model gave the closest values to the experimental thickness.

Higher consolidation values from the temperature profile are coming from the method overestimation when the temperature information is derived from the ridge block, not from the void. This effect is eliminated at the time of visit 4 because the consolidated layer reached the block bottom in the vertical profile of the thermistor (Fig. 16b). Similarly, there was no significant thickness overestimation in the range of 50–65 cm which corresponds to the void depth, measured during visit 1 (the ridge initial and final volumes. The initial ridge volume was estimated based on the measured volume of ice blocks, while the final ridge volume was estimated from its morphology at visit 4 (Fig. 8).

It is convenient to compare growth prediction from different models and experimental sources in one table (Table 2). Results of model application are quite similar for both types of ice: convective models are underestimating ice growth, while radiative models are giving values closer to experimental thicknesses.

It is of interest to evaluate thickness overestimation for the described experiment. We should assume as reference results of the numerical modelling using a radiative balance (Fig. 16b). As it was described for the general case, thickness overestimation mainly depends on ice temperature and its thickness (Fig. 17a). The first part of our experiment (days 0–35) with a thinner consolidated layer was performed at significantly lower air temperatures than the second part (days 35–66). The temperature effect on thickness overestimation was almost constant, and the scale effect was not considerable (Fig. 17b).

The calculated thickness overestimation was in the range of 0–25 cm or 0–5 cm/°C with a significant drop when the consolidated layer was growing in voids.

5. Discussion

5.1. Validation of consolidation models

There are two main options for validation of a model using field experiments in ridge consolidation: to compare temperature profiles or coring profiles. The accuracy of both methods is influenced by the inhomogeneity of the bottom surface of the consolidated layer. As was observed in previous studies (Blanchet, 1998; Høyland, 2002b; Timco and Burden, 1997), the consolidated layer thickness measurements from coring have too large variability and errors to be suitable for

consolidation model validation. Høyland (2002a) reported a 26% difference in consolidated layer thickness measurements performed by drilling and by temperature profile analysis. Timco and Burden (1997) analyzed maximum, minimum and average thickness of the consolidated layer for 25 ridges and found thickness variability larger than 3. This study attempted to show limitations and errors which can be observed in the analysis of ridge temperature and estimated thickness.

Consolidated layer thickness, as the key engineering parameter of an ice ridge, is one of the most important outputs of any fieldwork or modelling. Meanwhile, any consolidation model can give a value of minimum thickness not including the thickness of ice blocks, partly frozen into a consolidated layer. Because of that a simple condition of an ice and water boundary, where the temperature is equal to the water freezing point, would give thickness including ice blocks, inside which ice temperature is exponentially approaching freezing temperature. This condition is impractical because it is not providing values of interest (minimum consolidated layer thickness) and it also requires accurate equipment to distinguish small temperature differences. As it was shown in the paper, it is possible to use more advanced conditions of the ice-water interface, but even such algorithms can give overestimated values of consolidated layer thickness.

Another way to validate the consolidation model is to compare values of vertical heat fluxes or corresponding vertical temperature gradients. But heat flux is affected by local conditions much more than thickness. And to analyse the temperature profile, it is important to know its exact location, which is especially complicated for underwater ridge parts. Vertical heat flux under sail, below upper 20 cm affected by daily temperature deviations, and above bottom part of the consolidated layer can give a good estimate of heat transfer after the initial phase of consolidation. It is important to consider that large-scale ridges are not homogenous media and because of that heat fluxes are not only converting in vertical ice growth but also horizontal growth and thermal inertia.

As a conclusion, one should consider that thickness estimation from a temperature profile is more complicated for ridges and can give significant errors. At the same time, measured heat fluxes are also not always equal to the latent heat fluxes related to the change of consolidated layer thickness.

Radiative models are predicting faster ice growth under any conditions. Meanwhile, the difference between radiative and convective models' predictions can be significantly lowered due to the presence of the shortwave radiation. This explains why both radiative and convective numerical models accurately predict ice growth.

5.2. Thickness overestimation

At the level of minimum consolidated layer thickness, the

temperature in the surrounding ice blocks can be significantly colder depending on their distance from the block center. The thermistor string for the described experiment was placed in the ice block. From Fig. 16b it can be seen, that thickness values from the temperature profile are always approximately 15 cm larger than of analytical solution, while vertical heat fluxes in fully consolidated parts are almost equal for both the experiment and the model.

The heat fluxes in level ice and the consolidated layer below water level were almost equal during the first 25 days of the experiment when the snow thickness above both types of ice was in the same range. Level ice thickness and corresponding thermal resistance were higher only during the first 12 days. It shows the importance of coupling of air convection and conduction through snow and ice.

Even though thickness estimation with a smaller threshold is giving overestimated values, it is still preferable over usage of only temperature measurements from the top part of the consolidated layer. Accuracy of such a method is highly dependent on the accuracy of the temperature measuring device and even small error can lead to high errors in thickness.

Another uncertainty to be considered is the 2-in. drilling diameter of a borehole for the thermistor. The presence of such unfrozen void around thermistor can decrease values of thickness overestimation and to make temperature profile analysis more complicated. During the consolidation process, such a void will be frozen only after a front of significant temperature gradients reached that part of the drill hole. This can explain slightly lower thickness overestimation in our experiment in comparison to the numerical model result since it is not considering the presence of any voids around the virtual thermistor.

When first-year ridges get older approaching the melt season, the keel changes so that it becomes less porous and more homogeneous. This process will reduce the thickness overestimation and the different temperature distributions in voids and blocks.

5.3. Ice salinity

The increasing trend of level ice salinity can be explained by the presence of approximately 12 cm thick part of superimposed ice at the beginning of the experiment. This layer was potentially formed during the warm temperature period two weeks before the start of our experiment, on February 5–11, 2017, due to snow melt and later refreezing. The average daily air temperatures during that period were in the range 2.0–3.8 °C. The decreasing portion of less saline superimposed ice can explain the increase of level ice salinity with time.

Slightly lower ridge salinity in comparison to level ice can be explained by stronger ice desalinization after warming during the initial phase according to the brine dynamics model by Griewank and Notz (2013). It is well known that the initial salinity of the first year ice depends on the its growth rate (Kovacs, 1996). Vertical heat fluxes were almost equal in the consolidated layer and in level ice during the first 25 days when the upper 70 cm of the consolidated layer was formed. Ridge multi-directional desalinization process requires further investigations.

We observed a significant ice growth between visits 3 and 4 during relatively warm temperatures (Fig. 16): 27% of level ice thickness change occurred together with 35% of FDD, increased solar radiation, and relatively thick snow. According to our modelling results, it was

partly caused by the growth of the ice microporosity during its warming, which depends on its salinity. Similar growth was not observed at the modelling results with a thermodynamic model of fresh ice.

6. Summary and conclusions

A medium-scale sea ice ridge was produced in the Van Mijenfjorden, Svalbard in the winter of 2017. The thickness and properties of the level ice that was used to make the ridge were measured and thermistor-strings were installed in the ridge and the neighboring level ice. The ridge was visited four times for drilling and sampling. The experimental results provided enough information for accurate growth prediction and validation of ridge consolidation models.

Two analytical resistive models and two-dimensional discretized numerical models are presented. All models need general met-ocean conditions and general ice physical properties. The ridge models include the effect of the inhomogeneous top and bottom surfaces of the consolidated layer. The models were validated against the field measurements, and the furthers details of the analytical models were validated against the numerical model.

The main conclusion is:

- The analytical resistive ridge model with convective atmospheric flux captures the relevant phenomena well and could be used for prediction of the consolidated layer thickness in probabilistic analysis of ice actions on structures.

Additional important results and conclusions are:

- During our field experiment, the level ice grew from 50 to 99 cm, the consolidated layer grew up to 120 cm, and the macroporosity was about 0.36.
- The model including the radiative terms predicted heat fluxes in level ice and ridge better than the convective model but required more input data.
- Vertical temperature profiles through the consolidated layer and further into respectively a void and an ice block may result in significantly different estimations of the consolidated layer thickness.
- The difference between fresh and saline ice growth is becoming significant only during the warming phase.

Declaration of Competing Interest

None.

Appendix A. Radiative model

The net longwave radiation from the ocean surface q_{LW} can be found as (Rosati and Miyakoda, 1988):

$$q_{LW} = -\delta\sigma T_a^3 \left(T_a \left(0.254 - \frac{0.0066}{132.22} e_a \right) (1 - C_l c) + 4(T_{as} - T_a) \right) \tag{27}$$

where $\delta = 0.95$ is the emissivity of the sea surface relative to the black body, σ is the Stefan-Boltzmann constant, e_a is the near-surface vapour pressure

at air ambient temperature T_a, $C_l = 0.8$ is the cloud coefficient, c is the fractional cloud factor.

Alternatively, the net longwave radiation can be calculated as (Maykut, 1986):

$$q_{LW} = \varepsilon\sigma T_{as}^4 - \varepsilon^*\sigma T_a^4 \tag{28}$$

where $\varepsilon = 0.99$ is the snow longwave emissivity, and ε^* is the effective emissivity for the atmosphere, which can be found as (Maykut, 1986):

$$\varepsilon^* = 0.7855(1 + 0.2232\ c^{2.75}) \tag{29}$$

The net shortwave radiation q_{SW} can be found as (Shine, 1984):

$$q_{SW} = (1-\alpha)\Phi_c \frac{S cos^2 Z}{0.0455 + 1.2cosZ + (1+cosZ)10^{-5}e_a} \tag{30}$$

where α is the albedo of ice or snow, Φ_c is the cloud correction factor, S is the solar constant, and Z is the solar zenith angle.

Cloud correction factor Φ_c can be calculated as (Laevastu, 1960):

$$\Phi_c = 1 - 0.6c^3 \tag{31}$$

Sensible and latent heat fluxes can be found as (Maykut, 1986):

$$q_s = \rho_a c_a C_s V_w (T_a - T_{as}) \tag{32}$$

$$q_e = 0.622\rho_a L_e C_e V_w (e_a - e_{s0})/P \tag{33}$$

where ρ_a is the density of the air, c_a is the specific heat of the air, C_s and C_e are the bulk transfer coefficients for sensible and latent heat, V_w is the wind speed at the reference height, L_e is the latent heat of vaporization, RH is the relative humidity, e_{s0} is the saturation vapour pressure at surface temperature T_{as}, P is the total atmospheric pressure.

The vapour pressure e can be expressed through the saturation vapour pressure e_s at the given temperature and relative humidity RH as:

$$e = \text{RH·}e_s \tag{34}$$

The saturation vapour pressure e_s at the given temperature T can be found as (Tsonis, 2007):

$$e_s = 611exp(19.83 - 5417/(T+273.15)) \tag{35}$$

The bulk transfer coefficients for sensible and latent heat C_s and C_e mainly depends on wind speed and the temperature difference between surface and air $T_{as} - T_a$. For surfaces warmer than air these coefficients are usually in the range of $(1...2) \cdot 10^{-3}$ for the elevation of 10 m (Smith, 1988).

Appendix B. Saline ice growth

Prediction of saline ice growth includes additional complications connected to its temperature-dependent latent and sensible heat. Thermal inertia for saline ice can be divided into specific heat of pure ice and brine, and change of solid fraction at different temperatures, which requires freezing or melting of pure ice inside sea ice. The sum of both effects can be presented via the enthalpy of sea ice:

$$H_{si} = -L_i m_i - m_i \int c_i dT - (1-m_i)\int c_b dT \tag{36}$$

Enthalpy values at different temperatures illustrate the difference from pure ice growth model: depending on ice temperature and salinity only a certain mass fraction should be frozen, while additional negative heat should be spent to adjust ice temperature to a certain temperature profile. The zero value of enthalpy can be chosen arbitrarily and assumed zero at sea ice freezing point.

The brine salinity of sea ice is equal to (Notz, 2005):

$$S_b = -1.2 - 21.8\cdot T - 0.919\cdot T^2 - 0.0178\cdot T^3 \tag{37}$$

The sea ice solid mass fraction can be found as:

$$m_i = 1 - \frac{S_i}{S_b} \tag{38}$$

The sea ice solid volume fraction can be found as (Notz, 2005):

$$v_i = \frac{1 - \frac{S_i}{S_b}}{1 + \frac{S_i}{S_b}\left(\frac{\rho_i}{\rho_b} - 1\right)} \tag{39}$$

The thermal conductivity of sea ice is equal to (Notz, 2005):

$$k_{si} = v_i k_i + (1 - v_i)k_b \tag{40}$$

The heat capacity of sea ice per unit mass c_{si} can be found as (Notz, 2005):

$$c_{si} = c_i - L_i\frac{\alpha S_i}{T^2} \tag{41}$$
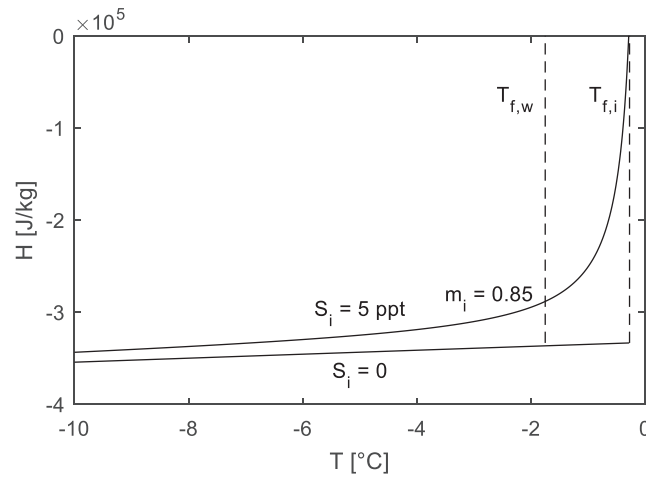
Fig. 18. Saline and fresh ice enthalpy vs temperature.

where $\alpha = -0.05411$ is the slope of the liquidus.

The density of sea ice was found as (Notz, 2005):

$$\rho_{si} = v_i\rho_i + (1 - v_i)\rho_b \tag{42}$$

The density of pure ice can be found from (Pounder, 1966) as:

$$\rho_i = 916.8 - 0.1403 \cdot T \tag{43}$$

The thermal conductivity of pure ice can be found from Eicken (2003); Yen et al. (1991) as:

$$k_i = 2.21 - 1.00 \cdot 10^{-2} T + 3.44 \cdot 10^{-5} T^2 \tag{44}$$

Pure ice heat capacity can be found as (Weast, 1977):

$$c_i = 2112.2 + 7.6973 \cdot T \tag{45}$$

The latent heat of fusion L_i of water is 333.5 kJ/kg (Feistel and Hagen, 1998). The enthalpy value for ice with any temperature and salinity distribution is defining how much energy should be extracted from the water for its consolidation and cooling (Fig. 18). As can be seen, enthalpy difference can be higher or lower than pure ice latent heat. Pure ice and brine sensible heat are decreasing sea ice growth at low temperatures in comparison to Stefan's equation. In contrast, the low solid fraction of warm sea ice can lead to faster growth in comparison to Stefan's equation and pure ice growth. For salinity of 5 ppt warm ice at water freezing temperature requires 15% less negative energy to be formed.

The difference between the top and bottom heat fluxes in ice is spent on ice heating or cooling. When ice is thick enough, the bottom heat flux depends only on average top surface temperature.

For the field data analysis, usage of the bottom ice boundary for heat flux calculation can be impractical due to high uncertainties in salinity and temperature profiles, while only the change of total ice volume is the main value of interest. The thickness of saline ice including sensible heat can be estimated from pure ice thickness without sensible heat from the solid volume fraction as:

$$h_{si} = h_i \frac{\rho_i L_i}{\rho_{si} \Delta H_{si}} \tag{46}$$

Appendix C. Extended surface theory

Any finned surface includes thermal conduction through the fin and thermal convection at its surfaces. Fin can be described by its width w and length l, which define two main parameters: top perimeter $P = 2(w + l)$ and top cross-section area $A_c = wl$. Heat transfer equation of a uniform fin cross-section in the vertical direction can be found as (Incropera et al., 2013):

$$\frac{d}{dz}\left(A_c\frac{dT}{dx}\right) - \frac{HP}{k_iA_c}(T - T_a) = 0 \tag{47}$$

This equation is convenient to present using dimensionless form using constant $m^2 = HP/k_iA_c$. To solve that equation boundary condition should be specified including the temperature at the base of the fin $T(0) = T_{base}$ and boundary condition at the top surface $HA_c(T(s) - T_a) = -k_iA_cdT/dx|_{z=s}$. Vertical heat flux through the sail is equal to (Incropera et al., 2013):

$$q_f = \sqrt{HPk_iA_c}(T_{base} - T_a)\frac{sinhms + (H/mk_i)coshms}{coshms + (H/mk_i)sinhms} \tag{48}$$

For analysis of temperature profiles, which are one of the primary measurements of any field experiments, it is also useful to know the temperature distribution above the consolidated layer, which can be expressed as (Incropera et al., 2013):

$$\frac{T - T_a}{T_{base} - T_a} = \frac{coshm(s - z) + (H/mk_i)sinhm(s - z)}{coshms + (H/mk_i)sinhms} \tag{49}$$

This equation can quantify the difference between heat flux at the water level and the snow-ice interface.

References

Adams, C.M., French, D.N., Kingery, W.D., 1960. Solidification of Sea Ice. J. Glaciol. 3, 745–761. https://doi.org/10.3189/S0022143000018050.

Blanchet, D., 1998. Ice loads from first-year ice ridges and rubble fields. Can. J. Civ. Eng. 25, 206–219. https://doi.org/10.1139/l97-073.

Calonne, N., Flin, F., Morin, S., Lesaffre, B., Du Roscoat, S.R., Geindreau, C., 2011. Numerical and experimental investigations of the effective thermal conductivity of snow. Geophys. Res. Lett. 38, 1–6. https://doi.org/10.1029/2011GL049234.

Cox, G.F.N., Weeks, W.F., 1983. Equations for determining the Gas and Brine Volumes in Sea-Ice Samples. J. Glaciol. 29, 306–316. https://doi.org/10.3189/S0022143000008364.

Eicken, H., 2003. From the microscopic to the macroscopic to the regional scale: Growth, microstructure and properties of sea ice. In: Thomas, D., Dieckmann, G.S. (Eds.), Sea Ice An Introduction to its Physics, Chemistry, Biology and Geology. Blackwell Science, London, pp. 22–81.

Feistel, R., Hagen, E., 1998. A Gibbs thermodynamic potential of sea ice. Cold Reg. Sci. Technol. https://doi.org/10.1016/S0165-232X(98)00014-7.

Førland, E.J., Hanssen-Bauer, I., Nordli, P.Ø., 1997. Climate Statistics and Longterm Series of Temperature and Precipitation at Svalbard and Jan Mayen. DNMI-Rapport, Klima.

Griewank, P.J., Notz, D., 2013. Insights into brine dynamics and sea ice desalination from a 1-D model study of gravity drainage. J. Geophys. Res. Ocean. 118, 3370–3386. https://doi.org/10.1002/jgrc.20247.

Høyland, K.V., 2002a. Simulations of the consolidation process in first-year sea ice ridges. Cold Reg. Sci. Technol. 34, 143–158. https://doi.org/10.1016/S0165-232X(02)00002-2.

Høyland, K.V., 2002b. Consolidation of first-year sea ice ridges. J. Geophys. Res. 107, 3062. https://doi.org/10.1029/2000JC000526.

Høyland, K.V., 2007. Morphology and small-scale strength of ridges in the North-western Barents Sea. Cold Reg. Sci. Technol. https://doi.org/10.1016/j.coldregions.2007.01.006.

Høyland, K.V., Jensen, A., Liferov, P., Heinonen, J., Evers, K.-U., Løset, S., Määttänen, M., 2001. Physical modelling of first-year ice ridges – part I: production, consolidation and physical properties. In: Proceedings of the 16th International Conference on Port and Ocean Engineering under Arctic Conditions, pp. 1483–1492.

Incropera, F.P., DeWitt, D.P., Bergman, T.L., Lavine, A.S., 2013. Principles of heat and mass transfer. Water. https://doi.org/10.1016/j.applthermaleng.2011.03.022.

Kovacs, A., 1996. Part I. Bulk Salinity Versus Ice Floe Thickness, 96. CRREL Rep, pp. 1–16.

Laevastu, T., 1960. Factors affecting the temperature of the surface layer of the sea. Comment. Phys. Math. 25.

Leppäranta, M., Hakala, R., 1992. The structure and strength of first-year ice ridges in the Baltic Sea. Cold Reg. Sci. Technol. 20, 295–311. https://doi.org/10.1016/0165-232X(92)90036-T.

Leppäranta, M., Lensu, M., Kosloff, P., Veitch, B., 1995. The life story of a first-year sea ice ridge. Cold Reg. Sci. Technol. 23, 279–290. https://doi.org/10.1016/0165-232X(94)00019-T.

Marchenko, A., 2008. Thermodynamic consolidation and melting of sea ice ridges. Cold Reg. Sci. Technol. 52, 278–301. https://doi.org/10.1016/j.coldregions.2007.06.008.

Maykut, G.A., 1986. The surface heat and mass balance. In: The Geophysics of Sea Ice. Springer US, Boston, MA, pp. 395–463. https://doi.org/10.1007/978-1-4899-5352-0_6.

Millero, F.J., 2010. Equation of State of Seawater. Oceanography 23, 18–33. https://doi.org/10.5670/oceanog.2010.21.COPYRIGHT.

Notz, D., 2005. Thermodynamic and Fluid-Dynamical Processes in Sea Ice. University of Cambridge.

Petrich, C., Langhorne, P.J., Haskell, T.G., 2007. Formation and struture of refrozen cracks in land-fast first-year sea ice. J. Geophys. Res. Ocean. 112, 1–13. https://doi.org/10.1029/2006JC003466.

Pounder, E.R., 1966. The Physics of Ice. Am. J. Phys. https://doi.org/10.1119/1.1973537.

Rosati, A., Miyakoda, K., 1988. A general circulation model for upper ocean simulation. J. Phys. Oceanogr. 18, 1601–1626. https://doi.org/10.1175/1520-0485(1988)018<1601:agcmfu>2.0.co;2.

Salganik, E., Høyland, K.V., 2018. Thermodynamics and consolidation of fresh ice ridges for different scale and configuration. In: Proceedings of 24th IAHR International Symposium on Ice.

Salganik, E., Høyland, K.V., Maus, S., 2020. Consolidation of fresh ice ridges for different scales. Cold Reg. Sci. Technol. 171 https://doi.org/10.1016/j.coldregions.2019.102959.

Sand, K., Winther, J.G., Maréchl, D., Bruland, O., Melvold, K., 2003. Regional variations of snow accumulation on Spitsbergen, Svalbard, 1997-99. Nord. Hydrol. https://doi.org/10.2166/nh.2003.0026.

Schwerdtfeger, P., 1963. The thermal Properties of Sea Ice. J. Glaciol. 4, 789–807. https://doi.org/10.1017/S0022143000028379.

Shestov, A., Høyland, K., Ervik, Å., 2018. Decay phase thermodynamics of ice ridges in the Arctic Ocean. Cold Reg. Sci. Technol. 152, 23–34. https://doi.org/10.1016/j.coldregions.2018.04.005.

Shine, K.P., 1984. Parametrization of the shortwave flux over high albedo surfaces as a function of cloud thickness and surface albedo. Q. J. R. Meteorol. Soc. https://doi.org/10.1002/qj.49711046511.

Smith, S.D., 1988. Coefficients for sea surface wind stress, heat flux, and wind profiles as a function of wind speed and temperature. J. Geophys. Res. Ocean. 93, 15467–15472. https://doi.org/10.1029/JC093iC12p15467.

Sturm, M., Holmgren, J., König, M., Morris, K., 1997. The thermal conductivity of seasonal snow. J. Glaciol. 43, 26–41. https://doi.org/10.1017/S0022143000002781.

Timco, G.W., Burden, R.P., 1997. An analysis of the shapes of sea ice ridges. Cold Reg. Sci. Technol. https://doi.org/10.1016/S0165-232X(96)00017-1.

Timco, G.W., Goodrich, L.E., 1988. Ice rubble consolidation. Proc. 9th Int. Symp. Ice. Int. Assoc. Hydraul. Eng. 1, 537–548.

Tsonis, A.A., 2007. An Introduction to Atmospheric Thermodynamics, an Introduction to Atmospheric Thermodynamics. Cambridge University Press, Cambridge. https://doi.org/10.1017/CBO9780511619175.

Weast, R.C., 1977. CRC Handbook of Chemistry and Physics, 57th edition (Handbook of Chemistry and Physics).

WMO Sea-Ice Nomenclature, 1971. J. Hydrol. https://doi.org/10.1016/0022-1694(71)90048-5.

Yen, Y.C., Cheng, K.C., Fukusako, S., June 11–14 1991. Review of intrinsic thermophysical properties of snow, ice, sea ice, and frost. In: Zarling, J.P., Faussett, S.L. (Eds.), Proceedings 3rd International Symposium on Cold Regions Heat Transfer, Fairbanks, AK. University of Alaska, Fairbanks, US, pp. 187–218.